

Wake Effects on Drift in Two-Dimensional Inviscid Incompressible Flows

Sergei Melkounian

*School of Computational Science and Engineering,
McMaster University
Hamilton, Ontario L8S4K1, CANADA*

Bartosz Protas*

*Department of Mathematics & Statistics,
McMaster University
Hamilton, Ontario L8S4K1, CANADA*

(Dated: November 4, 2021)

This investigation analyzes the effect of vortex wakes on the Lagrangian displacement of particles induced by the passage of an obstacle in a two-dimensional incompressible and inviscid fluid. In addition to the trajectories of individual particles, we also study their drift and the corresponding total drift areas in the Föppl and Kirchhoff potential flow models. Our findings, which are obtained numerically and in some regimes are also supported by asymptotic analysis, are compared to the wakeless potential flow which serves as a reference. We show that in the presence of the Föppl vortex wake some of the particles follow more complicated trajectories featuring a second loop. The appearance of an additional stagnation point in the Föppl flow is identified as a source of this effect. It is also demonstrated that, while the total drift area increases with the size of the wake for large vortex strengths, it is actually decreased for small circulation values. On the other hand, the Kirchhoff flow model is shown to have an unbounded total drift area. By providing a systematic account of the wake effects on the drift, the results of this study will allow for more accurate modeling of hydrodynamic stirring.

Keywords: drift; wakes; Föppl flow; Kirchhoff flow

* Corresponding author, Email: bprotas@mcmaster.ca

I. INTRODUCTION

When a body passes through an unbounded fluid, it induces a net displacement of fluid particles. The difference between the initial and final positions of a fluid particle is defined as the particle’s “drift” [1], and plays an important role in characterization of the stirring occurring in multiphase flows [2] and due to swimming bodies [3]. Hereafter we will exclusively focus on flows with velocity fields stationary in a suitable steadily translating frame of reference, and will consider flows symmetric with respect to the flow centerline. Analysis of drift in time-dependent flows is more involved and some efforts in this direction have been made using methods of chaotic dynamics [4, 5].

Following the seminal study by Munk [6], the phenomenon of drift has recently received a lot of attention in the context of mixing in the oceans caused by swimming organisms [7]. However, most of the theoretical descriptions of stirring rely on irrotational flow models used to compute or estimate the drift (an exception to this is a recent study [8] focused on the Stokesian approximation). The goal of the present contribution is to understand the effect of vortex wakes on the drift in inviscid flows. This will be accomplished in the two-dimensional (2D) setting using a combination of careful numerical computations and mathematical analysis. The set-up of the problem is illustrated in Figure 1 with (r, θ) and (r', θ') representing, respectively, the polar coordinates in the fixed and moving frame of reference.

Drift has been investigated for over a century with the earliest work belonging to Maxwell [9] who showed that, when the passing object is a circular cylinder inducing a simple potential flow, then surrounding fluid particles follow trajectories in the form of “elastica” curves (a more modern account of this problem can be found in monograph [10]). For a given fluid particle, an elastica-shaped trajectory approaches a straight line parallel to the path of the moving cylinder for points far upstream and downstream, and exhibits a loop with a fore-and-aft symmetry (when the particle travels along this loop, the cylinder is underneath it). The historical origins and some other applications of elasticas are surveyed in [11]. Another major contribution to this area is due to Darwin who, in addition to particle trajectories, studied the problem of drift area and drift volume which are global quantities characterizing the particle drift in a given flow. Darwin’s proposition [12], also referred to as a “theorem”, is a key result relating the drift area or volume of a moving body to its added mass. Its utility consists in the fact that the latter quantity tends to be easier to evaluate for flows past objects with complex shape. There has been some debate [13–16] concerning a rigorous proof of this result in its full generality which was centered on the evaluation method for conditionally convergent integrals. The relation between drift volume and added mass was investigated in a controlled experiment [17] where it was found that the shape of the displaced material surface is similar to that of the inviscid case and that the added mass coefficient measured for a spherical bubble for Reynolds numbers ranging from $Re = 500$ to 1000 is consistent with its value obtained from Darwin’s theorem. Connections between the Darwinian drift and the Stokesian drift, related to the wave motion, were explored in [18].

The concept of drift was recently generalized for the case of flows induced by propagating vortices (vortex rings) in [19]. Motivated by biofluid applications, recent studies [8, 20] investigated the effects of vortex wakes on the drift induced by simple swimmers moving in the Stokes fluid. On the other hand, recognizing that the concept of drift is idealized, in the sense that the object is assumed to travel during infinite time, corrections resulting from finite travel times were obtained leading to the definition of *partial drift* [16, 21]. This quantity was studied in recent experimental investigations concerning stirring by swimmers [7, 19]. Another related quantity is the mean squared displacement of particles which can be used to compute the effective diffusivity [3]. In the present study we provide a thorough account of the effects of different vortex wakes on the drift in inviscid flows. We will focus on 2D flows, because they offer simple solutions amenable to straightforward analysis, so that closed-form results can be obtained.

In our paper we begin in Section II by precisely defining the drift and the total drift area, and explaining how these quantities can be evaluated in a given flow. Then, in Section III, we introduce the different vortex flows considered in our study and identify their key parameters. Computational results are presented in Section IV together with a validation of the numerical approaches, whereas their discussion and a posteriori justification via asymptotic analysis are offered in Section V. Conclusions and outlook are deferred to Section VI.

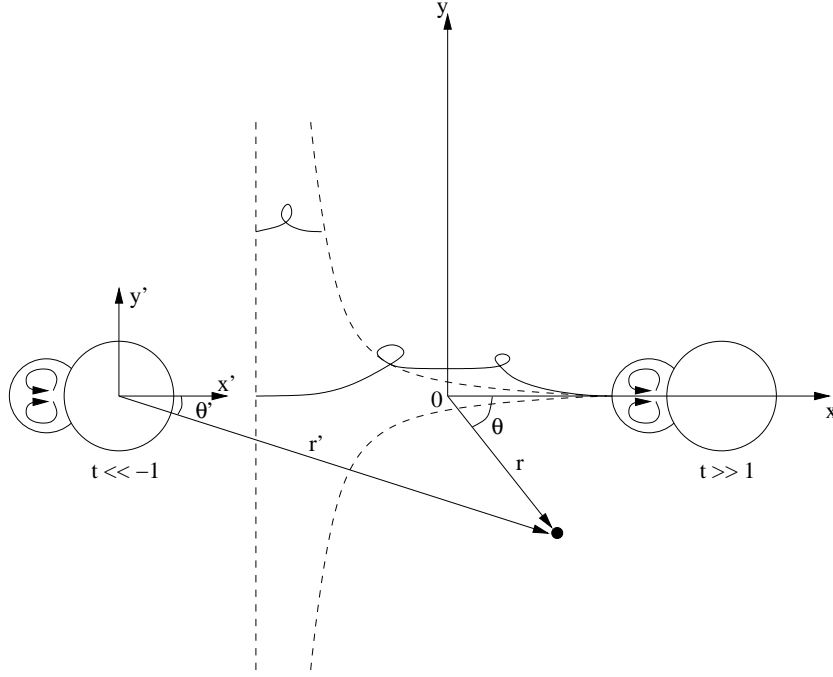


Figure 1: Schematic of the problem indicating representative particle trajectories and the coordinate systems used.

II. DRIFT: DEFINITION AND CALCULATION

We will consider a circular cylinder of unit radius ($a = 1$) passing through an incompressible inviscid fluid of unit density in a 2D unbounded domain Ω . We assume that the induced flow is potential and the cylinder passes with its center along the x -axis from $x = -\infty$ to $x = \infty$ with constant unit speed. Hence, in the cylinder's frame of reference there is a uniform stream at infinity such that $\mathbf{u} \rightarrow U\hat{\mathbf{x}}$ as $|\mathbf{x}| \rightarrow \infty$, where $U = -1$ and $\hat{\mathbf{x}}$ is the unit vector associated with the x -axis. In this frame of reference, the flow is steady, i.e., $\mathbf{u} = \mathbf{u}(\mathbf{x})$, and satisfies the no through-flow boundary condition $\mathbf{u} \cdot \mathbf{n} = 0$ on the cylinder boundary $\partial\Omega$, where \mathbf{n} is the unit normal vector. Euler system describing the flow is known to admit nonunique solutions and different such solutions will be discussed below.

Hereafter, without the risk of confusion, we will interchangeably use the vector and complex notation for various vector quantities. A point $(x, y) \in \Omega$ will be represented as $\mathbf{x} = [x, y]^T$ or $z = x + iy$, where $i := \sqrt{-1}$ (the symbol “:=” defines the quantity on the left-hand side with the quantity on the right-hand side). The fluid velocity will be denoted $\mathbf{u}(\mathbf{x}) = [u_x, u_y]^T$ or $V(z) = (u_x - iu_y)(z)$, where u_x and u_y are the x and y components. Assuming that the velocity field is incompressible and irrotational, it will be expressed in terms of the complex potential $W(z) = (\phi + i\psi)(z)$ as $V(z) = dW/dz$, where ϕ and ψ are, respectively, the scalar potential and the streamfunction.

In much the same way that Maxwell [9] and Darwin [12] studied the problem of drift, we will consider the trajectories and drifts of individual particles in the fluid as the cylinder passes. Let the initial position of the particle at $t = 0$ be \mathbf{x}_0 and $[x(t; \mathbf{x}_0), y(t; \mathbf{x}_0)]^T$ denote the corresponding particle trajectory. Then, the displacement, or *drift*, of the particle initially at \mathbf{x}_0 is defined as

$$\xi(\mathbf{x}_0) := \int_{-\infty}^{\infty} u_x(x(t; \mathbf{x}_0), y(t; \mathbf{x}_0)) dt, \quad (1)$$

where the horizontal velocity component u_x is given in the absolute frame of reference. Integral (1) is improper and the question of its convergence will be addressed further below. By changing the integration variable from time t to the polar angle θ' in the moving frame of reference, cf. Figure 1,

it can be transformed to an integral (still improper) defined over a finite interval $\theta' \in [0, \pi]$ with the bounds corresponding to the position of the particle in front and behind the obstacle. Rewriting the velocity in the polar coordinate system in the moving frame of reference as $\mathbf{u} = u_r \hat{\mathbf{r}}' + u_\theta \hat{\boldsymbol{\theta}}'$, where $\{\hat{\mathbf{r}}', \hat{\boldsymbol{\theta}}'\}$ are the two unit vectors, we may reformulate (1) as

$$\xi(\mathbf{x}_0) := \int_0^\pi r' \frac{u_x(r', \theta')}{u_\theta(r', \theta')} d\theta'. \quad (2)$$

Form (2) is more convenient for some of the manipulations we will need to perform when deriving the drift in wakeless flow (Section III A).

Historically, one of the quantities of interest in practical applications has been the *total drift area* D representing the integral displacement of particles initially located on a line perpendicular to the path of the obstacle at an infinite upstream distance (Figure 1)

$$D := 2 \int_0^\infty \xi(y_\infty) dy_\infty = \int_{-\infty}^{+\infty} \xi(\psi) d\psi, \quad (3)$$

where y_∞ is the transverse coordinate of the particle's position when $t \rightarrow -\infty$ (with a slight abuse of notation, ξ may be equivalently considered a function of \mathbf{x}_0 , y_∞ or ψ). The two integrals in (3) are equal, because $\psi \rightarrow y_\infty$ as $x \rightarrow \infty$. The total drift area D involves two nested improper integrals (in expressions (1) and (3)). Whether this quantity is actually well-defined has been the subject of a debate [13–16] with the conclusion that this is indeed the case, provided the order of integration is as used here, i.e., first with respect to the streamwise coordinate and then with respect to the transverse coordinate. On the other hand, reversing the order of integration will result in a conditionally convergent expression.

There are two ways to evaluate the total drift area D . First, we can use a suitably transformed definition of formula (3) combined with the particle displacement given in (1). From the practical point of view, the most convenient way to evaluate the improper integral (1) is to set the particle positions \mathbf{x}_0 at $t = 0$ and then obtain the trajectories by integrating the system

$$\frac{d\mathbf{x}(t)}{dt} = \mathbf{u}(\mathbf{x}(t)), \quad \mathbf{x}(0) = \mathbf{x}_0 \quad (4)$$

forward and backward in time, i.e., for $t \rightarrow \pm\infty$, for different \mathbf{x}_0 . Since the initial particle positions in formula (3) are given at infinity, they need to be transformed to positions with finite streamwise locations, e.g., $\mathbf{x}_0 = [0, y_0]^T$. Since for a particle on a given streamline, ψ is constant and equal to some C , we have

$$C = \psi(0, y_0) = \lim_{x \rightarrow \infty} \psi(x, y_\infty) = y_\infty. \quad (5)$$

Defining $g(y_0) := \psi(0, y_0) = y_\infty$ as the map between the y -coordinates of the particle at $x = 0$ and at $x = \infty$, we obtain

$$\frac{dy_\infty}{dy_0} = g'(y_0), \quad (6)$$

so that (3) becomes

$$D = 2 \int_1^\infty \xi(g(y_0)) g'(y_0) dy_0, \quad (7)$$

where the lower bound is now set to unity, because the particle on the streamline with $\psi = 0$ has the coordinate $y_0 = 1$ at $x_0 = 0$. We note that function $g(y_0)$ will be different for different solutions of the Euler equations governing the flow problem.

The second method to evaluate the total drift area is to use Darwin's theorem [12] which stipulates that $D = M$, where M is the added mass, and the fluid density is assumed equal to the unity. For our

problem, the added mass is given by a line integral over the contour \mathcal{C} which is the boundary of the largest region with closed streamlines

$$M = \oint_{\mathcal{C}} \phi n_x ds, \quad (8)$$

where n_x is the x -component of the unit normal vector. In addition to the boundary of the obstacle, contour \mathcal{C} also comprises the boundary of the recirculation region, if it is present in the flow. The reason is that, in obtaining relation (8), the divergence theorem cannot be applied on regions where singularities (point vortices) are present.

Alternatively, one can bypass evaluation of integral (8) by the application of Taylor's added mass theorem [22]. If we consider the union of our cylinder and the recirculation region as a single "body" \mathcal{B} in motion, this theorem allows us to compute the added mass in terms of the singularities within this region. Suppose that our composite body contains N sources and sinks with locations z_i and strength m_i . In addition, it contains M doublets (or dipoles) with strength μ_j and continuously distributed sources and sinks with area density defined by σ . Then for irrotational flows, the generalized form of the added mass given in [23] is

$$A_{\alpha 1} + B_{\alpha 1} + i(A_{\alpha 2} + B_{\alpha 2}) = 2\pi\rho \left[\int_{\mathcal{B}} \sigma_{\alpha} z dA + \sum_{i=1}^N m_{i\alpha} z_i + \sum_{j=1}^M \mu_{j\alpha} \right], \quad \alpha = 1, 2, \quad (9)$$

where A is the added mass tensor and B is a tensor representing the mass of the displaced fluid per unit area of the body with entries given by

$$B_{\alpha\beta} = \rho \oint_{\mathcal{C}} x_{\beta} n_{\alpha} ds, \quad \alpha, \beta = 1, 2 \quad (10)$$

in which $x_1 = x$, $x_2 = y$, $u_1 = u_x$, $u_2 = u_y$. For our problem, formula (9) simplifies quite significantly. In particular, since we are considering rectilinear motion in the x -direction of a body symmetric with the OX axis, we need only consider the element of the added mass tensor with $\alpha, \beta = 1$ so we may take the real part of (9) and drop these indices. Further, as there are no continuous sources or sinks and $\rho = 1$, we get for the added mass (now writing $A = M$)

$$M = 2\pi \Re \left[\sum_{i=1}^N m_i z_i + \sum_{j=1}^M \mu_j \right] - B. \quad (11)$$

In addition, since ds is a infinitesimal distance along the body, we have $n_x ds = dy$. Thus, B can be simplified and interpreted as the area of the cylinder augmented by the area of the wake

$$B = \oint_{\mathcal{C}} x n_x ds = \oint_{\mathcal{C}} x(y) dy. \quad (12)$$

We remark that relation (11) can be interpreted as consisting of two parts: a "universal" part represented by the first term involving only the far-field expansion of the velocity field induced by the obstacle together with its vortex system and a second part characterizing the specific flow and represented by B . An analogous decomposition of the total drift area was obtained in [8] for a swimmer in the Stokes flow. While all three approaches, involving definition formula (3), added-mass relation (8) and Taylor's theorem (11)–(12), are equivalent as far as the evaluation of the total drift area is concerned, the first one offers additional insights in the form of the particle trajectories responsible for the observed drift.

III. MODEL PROBLEMS

In this Section we describe the three model flows we will consider in our study. In addition to the wakeless potential flow for which the questions of drift are well understood and which will serve as a reference, we will also investigate the Föppl and Kirchhoff flows which will be shown to have quite different properties. These two flows are often invoked as the possible inviscid limits of steady viscous Navier-Stokes flows [24]. For simplicity, in all three cases the cylinder radius and the free stream at infinity have unit values, $a = 1$ and $U = -1$.

A. Wakeless Potential Flow

In the frame of reference attached to the obstacle, this flow is defined by the complex potential

$$W(z) = -\left(z + \frac{1}{z}\right) \quad (13)$$

which does not involve any parameters. The flow field exhibits no separation and is characterized by symmetry with respect to both OX and OY axes. The streamline pattern is illustrated in Figure 3a.

B. Föppl Flow

The Föppl vortex system [25] is a one-parameter family of solutions constructed by superimposing a pair of opposite-sign vortices with circulations $\Gamma > 0$ and $-\Gamma$ located symmetrically at $z_1 = x_1 + iy_1$, $y_1 > 0$, and \bar{z}_1 , where the overbar denotes complex conjugation, on the flow with potential (13). The resulting potential of the Föppl flow is thus

$$W(z) = -\left(z + \frac{1}{z}\right) + \frac{\Gamma}{2\pi i} \log\left(\frac{z - z_1}{z - \frac{1}{\bar{z}_1}}\right) - \frac{\Gamma}{2\pi i} \log\left(\frac{z - \bar{z}_1}{z - \frac{1}{z_1}}\right). \quad (14)$$

The locus of equilibrium vortex locations, the so-called Föppl curve, is described by the algebraic relation

$$r_1^2 - 1 = 2r_1 y_1, \quad (15)$$

where $r_1 := \sqrt{x_1^2 + y_1^2}$. The circulation of the vortices is related to their position through

$$\Gamma = 2\pi \frac{(r_1^2 - 1)(r_1^4 - 1)}{r_1^5}. \quad (16)$$

For a given circulation $\Gamma > 0$, the Föppl system is a limiting solution (as the vortex area goes to zero) of a family of Euler flows with finite-area vortex patches discovered by Elcrat et al. [26] (see also [27]). The Föppl system features a closed recirculation region with size growing with Γ . As is evident from (14), in the limit $\Gamma \rightarrow 0$ the wakeless potential flow from Section III A is recovered. The streamline patterns of Föppl flows with three representative values of the circulation Γ are illustrated in Figures 3b-d. The Föppl system has been successfully employed as a model in a number of studies concerning the stability and control of separated wake flows [28–32].

C. Kirchhoff Flow

The Kirchhoff flow is a manifestation of the free-streamline theory of the 2D ideal flows [33]. It features an object with two free streamlines in the upper and lower half-planes that separate the external fluid

from the region behind the object, called the cavity region, where the velocity is zero and the pressure is constant. Commonly, the object used for these types of flows is a flat plate, however, for consistency with the wakeless potential and the Föppl flows, we will consider here a 1st-order approximation of a circular cylinder presented in [34]. The Kirchhoff flow is interesting as an inviscid model, because it features an infinite wake and a finite drag.

We will first clarify the notation: variable z denotes the physical plane we are interested in, where the circular cylinder is of unit radius centered at $(0, 0)$ and the flow is moving from right to left, whereas variable Z refers to the physical plane as used in [34], where the cylinder instead has a radius of approximately 1.77 and is centered at approximately $(1.38, 0)$ with flow going in the opposite direction. We can define a map to switch between the two spaces

$$Z(z) := -1.770434824562303 \bar{z} + 1.377445608362303. \quad (17)$$

The complex potential is defined as a modified Levi-Civita transformation [34]

$$W(\tau) = -\frac{\left(\tau - \frac{1}{\tau}\right)^2}{4} \quad (18)$$

where $\tau = \rho e^{i\sigma}$ and $0 \leq \rho \leq 1$, $-\pi/2 \leq \sigma \leq \pi/2$. Unlike the models described in Sections III A and III B, potential (18) is not given in terms of the variable in the physical space and additional transformations are needed, so that it can be evaluated at z or Z . An intermediate map $\zeta(\tau)$ may be used to connect the τ and Z planes

$$\zeta = \frac{dZ}{dW} \quad (19)$$

and for a 1st-order approximation of a circular cylinder we have

$$\zeta(\tau) = \frac{1 + \tau}{1 - \tau} e^{-0.9426\tau + 0.0191\tau^3}. \quad (20)$$

Then, using the chain rule, we may write

$$\frac{dZ}{d\tau} = \frac{dZ}{dW} \frac{dW}{d\tau}, \quad (21)$$

where the first derivative factor is (20) and the second can be derived from (18). Thus, $Z(\tau)$ can be determined up to a constant through the integration

$$\begin{aligned} Z(\tau) &= \int_a^{\tau_0} \frac{dZ}{dW} \frac{dW}{d\tau'} d\tau' \\ &= -\frac{1}{2} \int_a^{\tau_0} \left(\frac{1 + \tau'}{1 - \tau'} \right) \left(1 + \frac{1}{\tau'^2} \right) \left(\tau' - \frac{1}{\tau'} \right) e^{-0.9426\tau' + 0.0191\tau'^3} d\tau' \end{aligned} \quad (22)$$

where τ_0 is an arbitrary constant. Integral (22) does not lend itself to analytical treatment, however, a generalized series expansion for the integrand was found up to $\mathcal{O}(\tau^2)$ around $\tau = 0$, so that, after integration, we obtain

$$Z(\tau) = -\frac{1}{2} (c_1 \tau^{-2} + c_2 \tau^{-1} + c_3 \log \tau + c_4 \tau + c_5 \tau^2) + Z_0, \quad (23)$$

where $c_1 = 0.5$, $c_2 = 1.0574$, $c_3 = -0.55904738$, $c_4 = -0.8828122332$, $c_5 = 0.1113906656$ and Z_0 is some constant.

>From (19) and (20), we can now compute the velocities in the Z -plane in terms of the τ variable

$$u_x(\tau) = \Re \left(\frac{1}{\zeta(\tau)} \right), \quad (24a)$$

$$u_y(\tau) = -\Im \left(\frac{1}{\zeta(\tau)} \right). \quad (24b)$$

Since we are interested in the flow in the direction opposite to the one in the Z -plane [34], we set $V(z) = (u_x - iu_y)(z) = (-u_x - iu_y)(\tau)$. In order to be able to evaluate velocities (24) at a given location Z in the physical space, we need to invert map (23), i.e., find $\tau = Z^{-1}(z)$. This is done by applying Newton's method to

$$F(\tau) = -\frac{1}{2}(c_1\tau^{-2} + c_2\tau^{-1} + c_3 \log \tau + c_4\tau + c_5\tau^2) - Z = 0. \quad (25)$$

Once τ is found, the velocity at the required location can be computed using (24). The streamlines of the Kirchhoff flow can be seen in Figure 3e.

IV. RESULTS

In this Section we compare the trajectories of individual particles, their drift and the corresponding total drift areas in the three flows introduced in the previous section. While, as reviewed below in Section IV A, these quantities can be determined analytically in the wakeless potential flow, they have to be computed numerically in the case of the Föppl and Kirchhoff flows, and the computational techniques are described and validated in Section IV B. Finally, the main results are presented in Section IV C.

A. Lagrangian Trajectories and Drift in the Wakeless Potential Flow

These classical results, recalled here for completeness, were derived by Maxwell [9] and were also surveyed in [10]. A key relation which makes this problem analytically tractable allows one to express the radial coordinate of the particle in the cylinder's frame of reference r' in terms of its azimuthal angle θ' with the streamfunction ψ used as a parameter

$$r'(\theta') = \frac{\psi + \sqrt{\psi^2 + 4a^2 \sin^2 \theta'}}{2 \sin \theta'}. \quad (26)$$

Then, when expressed using the angle η made by the tangent to the particle trajectory at a given point and the OX axis as the dependent variable and the arc-length s as the independent variable, the equation governing the particle trajectories is of the form

$$\frac{d\eta}{ds} = \frac{4}{a^2} \left(y - \frac{1}{2}\psi \right) \quad (27)$$

implying that the trajectories are examples of "elastica", a family of curves with a long history in mathematics [11]. The quantity $d\eta/ds$ represents the curvature of the trajectory and the connection with elastica was first recognized by Milne-Thomson [10]. However, for our purposes, it is more convenient to work with equation (2) where the independent variable is changed from t to θ' . Then, combining the resulting equation with relation (26) and integrating we obtain

$$x(u) = \frac{a}{k} \left[\left(1 - \frac{1}{2}k^2 \right) u - E(u) \right], \quad (28a)$$

$$y(u) = \frac{a}{k} \left[\frac{dk}{d\psi} + \text{dn}(u) \right], \quad (28b)$$

where $k := 2a/\sqrt{\psi^2 + 4a^2}$ (in our case $a = 1$),

$$E(u) := \int_0^{\theta' - \pi/2} \sqrt{1 - k^2 \sin^2 \theta} d\theta,$$

$$\text{dn}(u) := \sqrt{1 - k^2 \sin^2(\theta' - \pi/2)}$$

which are, respectively, an incomplete elliptic integral of the second type and a Jacobi elliptic function. The variable u parameterizing trajectories (28) is defined as an incomplete elliptic integral involving the polar angle θ' (Figure 1)

$$u := \int_0^{\theta' - \pi/2} \frac{1}{\sqrt{1 - k^2 \sin^2 \theta}} d\theta. \quad (29)$$

We note that the initial position of the particle is encoded in the value of the streamfunction ψ appearing in the expression for k . The drift corresponding to $t \in (-\infty, \infty)$, cf. (1) is then obtained by taking the limit $\theta' \rightarrow \pi/2$ in (28a) which yields, after setting $a = 1$ and noting (5),

$$\xi_1(y_0) = \frac{2}{k} \left[\left(1 - \frac{1}{2}k^2 \right) K - E \right], \quad (30)$$

where

$$K = \int_0^{\pi/2} \frac{1}{\sqrt{1 - k^2 \sin^2 \theta'}} d\theta', \quad E = \int_0^{\pi/2} \sqrt{1 - k^2 \sin^2 \theta'} d\theta'$$

are the complete elliptic integrals of the first and second type. Using Darwin's theorem, the total drift volume can then be shown to be

$$D_1 = \pi. \quad (31)$$

These results will be illustrated in Section IV C.

B. Numerical Computation of Particle Trajectories, Drift and Total Drift Area in the Föppl and Kirchhoff Flows

Since explicit relations of the type (26) are not available for the Föppl and Kirchhoff flows, we need to resort to numerical computations in order to determine the particle trajectories, drift and the total drift area. The particle trajectories are computed as described in Section II by solving system (4) with the initial data $\mathbf{x}_0 = [0, y_0]^T$, where $y_0 > 1$ is a parameter (we note that, when $y_0 = 1$ in Föppl flow, the particle is on the streamline connected to the stagnation point and the drift $\xi(1)$ is infinite). In the case of the Föppl flow the particle trajectories are additionally parameterized by the vortex circulation Γ . The velocity on the right-hand side of (4) is obtained, respectively, by complex-differentiating potential (14) and using expressions (24) in the two cases. System (4) is integrated for different values of y_0 and, in the case of the Föppl flow, Γ using MATLAB routines `ode23` and `ode45` with adaptive adjustment of the time step. Numerical evaluation of the drift, given by an improper integral (1), is a subtle issue requiring judicious choice of the truncation $[-T, T]$ of the original unbounded interval $(-\infty, \infty)$. As shown in [16, 21], such truncation of the integration domain leads to nontrivial corrections to the drift defined in (1) resulting in the so-called partial drift. In order to exclude these finite-time effects from the numerical integration, one has to make sure that T is chosen sufficiently large. For Föppl flow, this is achieved by setting T close to `realmax`, the largest positive floating-point number in the IEEE double-precision standard [35], which is of the order $\mathcal{O}(10^{300})$ and then balancing the accuracy with the computational time by adjusting the relative and absolute tolerances, `RelTol` and `AbsTol`, in the routines `ode23` and `ode45`. Owing to the adaptive adjustment of the time step employed in these routines, the total computational time required for a single particle trajectory does not typically exceed one minute on a state-of-the-art workstation even for the finest tolerances. This approach is validated by computing the particle trajectories $\mathbf{x}(t; y_0)$ and the associated drift $\xi(y_0)$ numerically for the wakeless potential flow (obtained setting $\Gamma = 0$ in (14)) and then comparing them to the analytical expressions (28) and (30) (since these formulas involve special functions, care must be taken to enforce a required level of precision in the evaluation of these functions as well). The results obtained for a single trajectory with $y_0 = 2$ are presented in Figure 2a, where we show a segment of the particle trajectory

computed numerically and given by expression (28), and in Figure 2b in which we show the difference between the exact drift value $\xi_1(2) = 2.011398641052742 \times 10^{-1}$ and its numerical approximation $\hat{\xi}_1(2)$ for different fixed `RelTol` and varying `AbsTol`. As is evident from Figure 2b, the error in the evaluation of the drift is rather small and decreases algebraically with the refinement of both `RelTol` and `AbsTol`. Thus, in all subsequent calculations we will use routine `ode45` with `RelTol` = `AbsTol` = 10^{-13} .

Unlike in the case of the wakeless and Föppl flow where T was allowed to extend close to `realmax`, in Kirchhoff flow we have to restrict the truncation of the time axis to $T = 10^3$ which is due to the failure of Newton's method applied to (25) to converge for such large values of t . However, since the structure of the flow advecting the particles does not change much when $|t| > T$, we will compensate for this by extrapolating the velocity for large times. Since, as will be shown below, the velocity field following the particle trajectory is for sufficiently large t a power-law function of time, this extrapolation will be performed using the formula

$$h(t) = ct^\beta, \quad (32)$$

where $c \in \mathbb{R}$ and $\beta < 0$, using 10 data points corresponding to the largest available times.

As regards evaluation of the total drift area D , three different approaches can be used: definition formula (3), or more conveniently (7), added-mass formula (8) and Taylor's theorem (11)–(12). In the first approach the parameter space y_0 is discretized in such a way that the relative variation of $\xi(y_0)$ between two adjacent discrete values of y_0 would not exceed 1%. The function $g(y_0)$ and its derivative needed in (7) are identified for the Föppl flow as follows

$$g(y_0) = -\left(y_0 - \frac{1}{y_0}\right) + \frac{\Gamma}{2\pi} \left[\log \left(\frac{\sqrt{x_1^2 + (y_0 + y_1)^2}}{\sqrt{x_1^2 + (y_0 - y_1)^2}} \right) + \log \left(\frac{\sqrt{\left(\frac{x_1}{x_1^2 + y_1^2}\right)^2 + \left(y_0 - \frac{y_1}{x_1^2 + y_1^2}\right)^2}}{\sqrt{\left(\frac{x_1}{x_1^2 + y_1^2}\right)^2 + \left(y_0 + \frac{y_1}{x_1^2 + y_1^2}\right)^2}} \right) \right], \quad (33)$$

$$g'(y_0) = -\left(1 + \frac{1}{y_0^2}\right) + \frac{\Gamma}{2\pi} \left[\frac{y_0 + y_1}{x_1^2 + (y_0 + y_1)^2} - \frac{y_0 - y_1}{x_1^2 + (y_0 - y_1)^2} + \frac{y_0 - \frac{y_1}{x_1^2 + y_1^2}}{\left(\frac{x_1}{x_1^2 + y_1^2}\right)^2 + \left(y_0 - \frac{y_1}{x_1^2 + y_1^2}\right)^2} - \frac{y_0 + \frac{y_1}{x_1^2 + y_1^2}}{\left(\frac{x_1}{x_1^2 + y_1^2}\right)^2 + \left(y_0 + \frac{y_1}{x_1^2 + y_1^2}\right)^2} \right]. \quad (34)$$

Concerning the computation of the total drift area via Taylor's theorem (11)–(12), the two Föppl vortices and their images inside the cylinder make the contributions $m = \pm \frac{\Gamma}{2\pi i}$ each, whereas the dipole at the origin contributes $\mu = Ua^2$. Therefore, after setting $a = 1$ and $U = -1$, equation (11) becomes

$$M = 2\pi \Re \left(\frac{\Gamma}{2\pi i} z_1 - \frac{\Gamma}{2\pi i \bar{z}_1} - \frac{\Gamma}{2\pi i} z_2 + \frac{\Gamma}{2\pi i \bar{z}_2} - 1 \right) - B \\ = -2\pi + 2\Gamma \left(y_1 - \frac{y_1}{x_1^2 + y_1^2} \right) - B. \quad (35)$$

Since it does not appear possible to find an analytic expression for B representing the area of the recirculation bubble, it has to be evaluated numerically using (12).

C. Comparison of Particle Trajectories, Drift and Total Drift Area in Flows with Different Wake Models

The particle trajectories corresponding to several different initial positions $\mathbf{x}_0 = [0, y_0]^T$ are shown in Figure 3 for the wakeless potential flow, the Föppl flow with different circulations Γ and for the

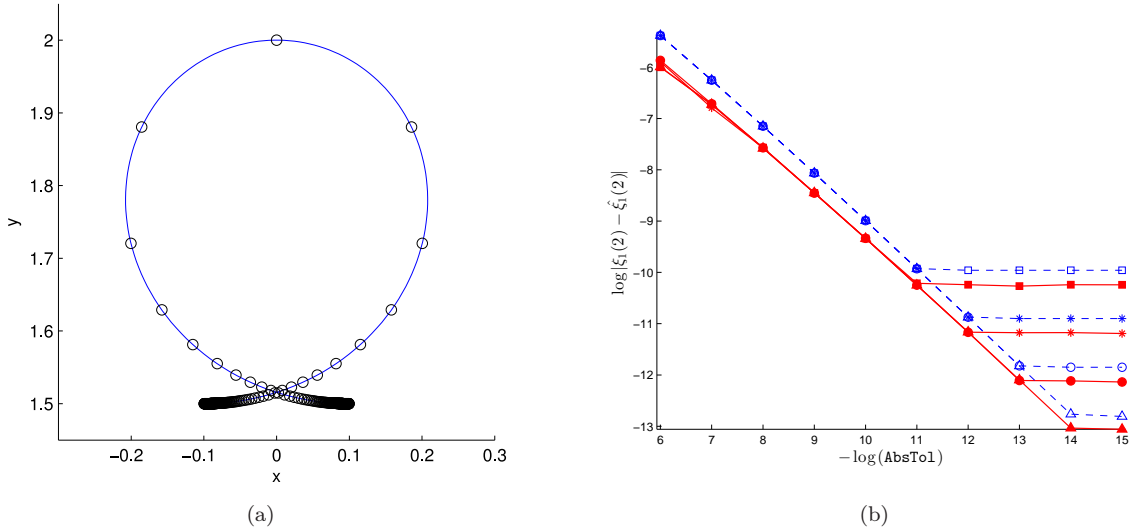
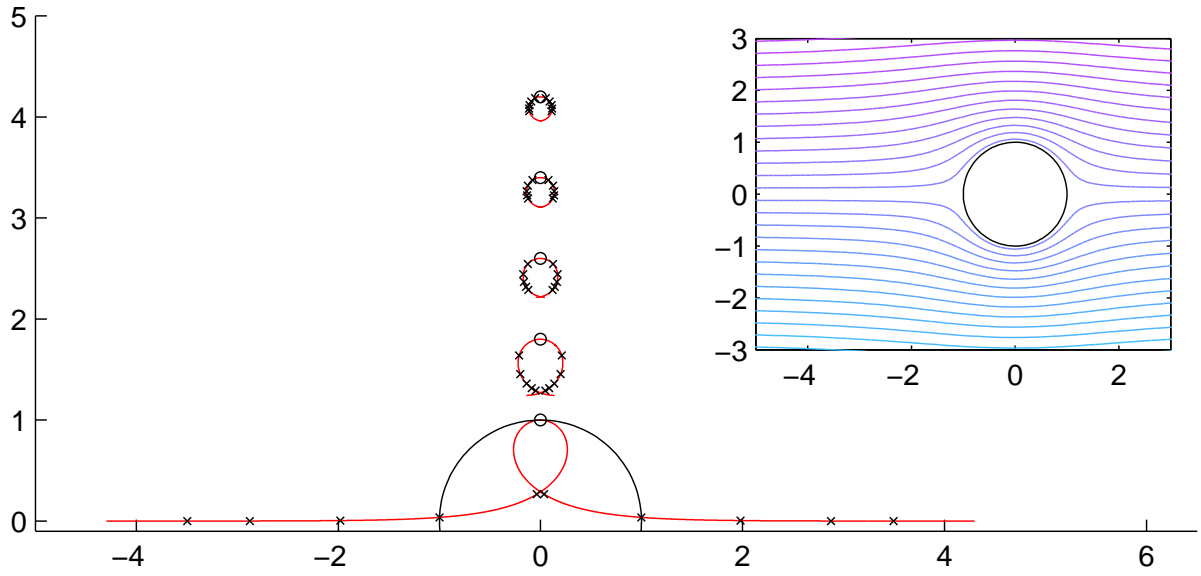


Figure 2: (a) Particle trajectories corresponding to $y_0 = 2$ in the wakeless potential flow obtained numerically with $\text{RelTol} = \text{AbsTol} = 10^{-13}$ (symbols) and evaluated analytically using formulas (28) (solid line); (b) error between the corresponding drift $\xi_1(2)$, cf. (30), and its numerical approximation $\hat{\xi}_1(2)$ computed using routines `ode23` (open symbols) and `ode45` (filled symbols) for $\text{RelTol} = 10^{-10}$ (squares), 10^{-11} (stars), 10^{-12} (circles), and 10^{-13} (triangles).

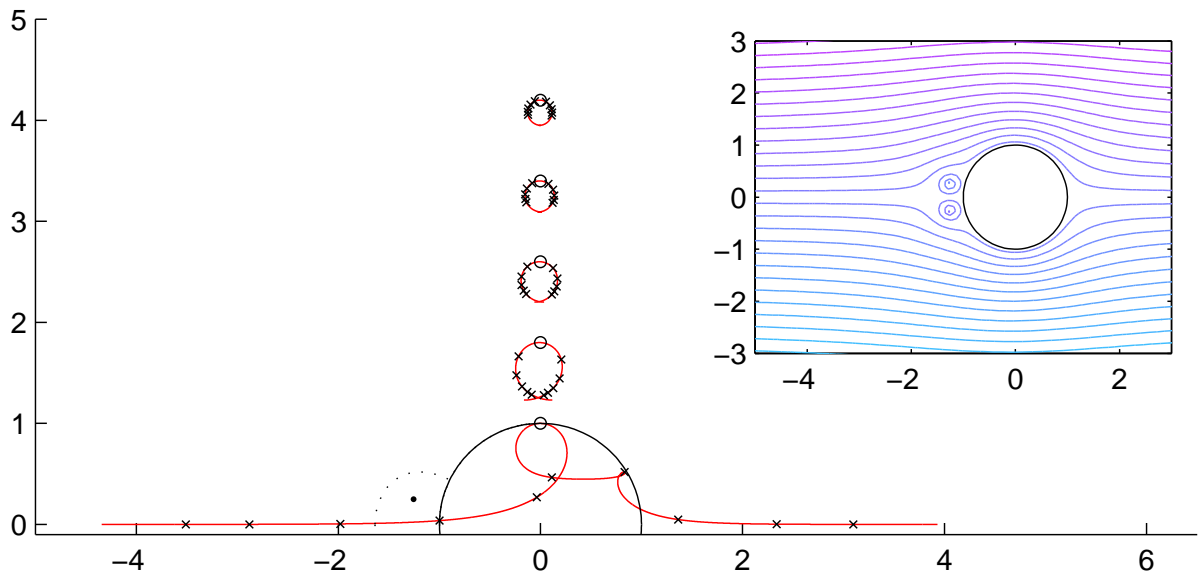
Kirchhoff flow (the wakeless potential flow is obtained as the Föppl flow with $\Gamma = 0$). The initial positions corresponding to the indicated cylinder locations are marked with circles, whereas crosses indicate the particle positions at the same instances of time in the different cases. First, we see that in the wakeless potential flow (Figure 3a) all the particle trajectories have the form of elastica curves symmetric with respect to the OY axis. The presence of the vortex wakes in the Föppl flows breaks the fore-and-aft symmetry of the trajectories and, for small values of y_0 , spawns a second loop on the trajectory which becomes larger for increasing vortex circulations Γ . The presence of this secondary loop results from the fact that, for sufficiently small y_0 , the transverse component u_y of the particle velocity must change sign when the particle is flowing around the recirculation region. Supplementary material, available on-line [36], contains animated versions of particle trajectories for a single particle close to the cylinder’s line of motion and for particles that are initially aligned vertically as indicated in Figure 1.

Next, in Figure 4a, we show the drift ξ of the individual particles as a function of the circulation Γ and, in Figure 4b, as a function of the initial distance y_0 form the horizontal axis. Since this is how it is often presented, the latter data is replotted in Figure 4c using the linear scaling with the drift ξ marked on the horizontal axis and the vertical axis representing y_∞ , cf. (5). In Figure 4a we see that the dependence of the drift ξ on the vortex circulation Γ is not monotonous regardless of the initial position of the particle. Moreover, in a certain range of Γ there are *two* initial positions y_0 such that the corresponding drift $\xi(y_0)$ is equal to the drift in the wakeless flow. While for sufficiently large circulations the drift ultimately increases as compared to the wakeless flow (corresponding to $\Gamma = 0$), for small values of Γ the drift is actually reduced. In other words, for every $y_0 > 1$ there exists a “critical” circulation $\Gamma_0 > 0$ such that the Föppl flow has the same drift ξ as the wakeless flow. This critical circulation is a nonmonotonous function of the distance y_0 from the flow centerline. In addition to confirming these observations, Figure 4b shows that drift $\xi(y_0)$ is a decreasing function of y_0 which exhibits two distinct asymptotic regimes (see Section V for more details on this).

It turns out that, regardless of the initial position $\mathbf{x}_0 = [0, y_0]^T$, in the Kirchhoff flow drift (1) is *unbounded*. This is evident from Figure 5 showing an extrapolation using formula (32) of the velocity component $u_x(t)$ following the particle trajectory for large positive and negative times. We observe



(a) wakeless potential flow ($\Gamma = 0$)



(b) $\Gamma = 1.9663$

Figure 3: Particle trajectories for different initial conditions $\mathbf{x}_0 = [0, y_0]^T$ in the wakeless potential flow (a), the Föppl flow with different circulations (b,c,d) and the Kirchhoff flow (e), with the insets illustrating the streamline patterns of the flows. The x's represent the particle positions at unit time intervals, whereas the o's correspond to the particle positions at $t = 0$, at which the cylinder, recirculation bubble for Föppl flow and the cavity for Kirchhoff flow are also indicated. The total drift areas produced by the fluid displacements shown in figures (a) and (c) are approximately equal, cf. (7), even though the individual particles with the same initial locations have quite different trajectories.

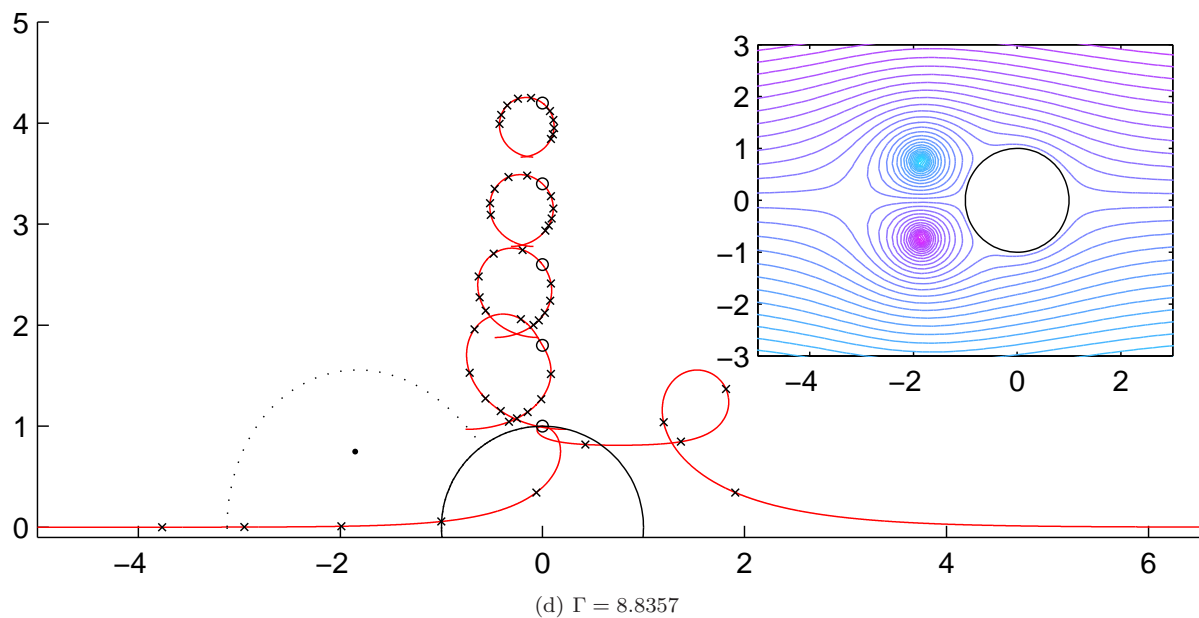
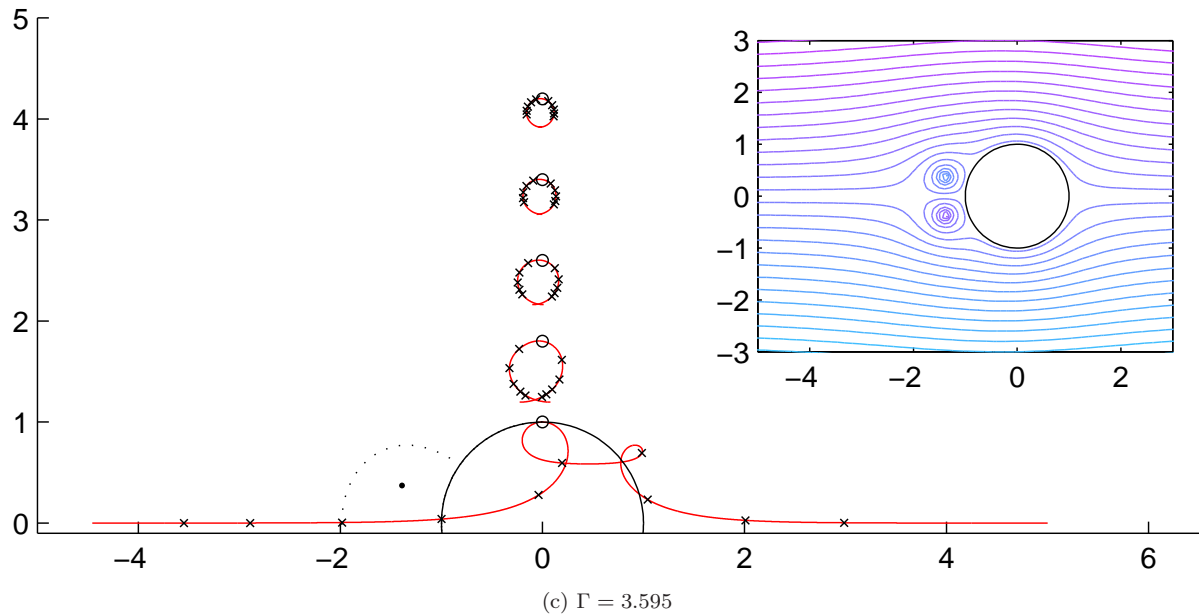


Figure 3: (Continued, see previous caption for details)

that, while for positive times the asymptotic behavior is characterized by the exponent $\beta = -1.1172$, for negative times the exponent is $\beta = -0.5092$ implying that $u_x(t)$ is not in fact integrable. Although for brevity in Figure 5 the data was shown for one trajectory only (corresponding to $y_0 = 5$), analogous results we also obtained for other trajectories. Thus, the drift data is not shown for the Kirchhoff flow in Figure 4.

Finally, in Figure 6, we show the dependence of the total drift area D on the vortex circulation Γ computed using the three methods discussed in Section IV B, all of which show excellent agreement. We

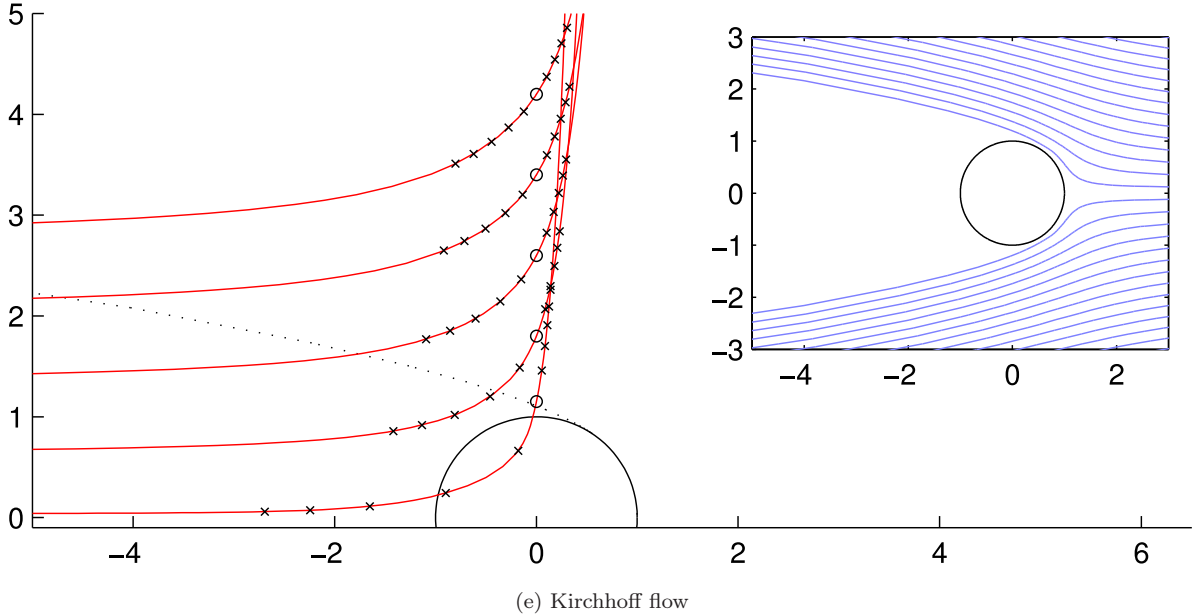


Figure 3: (Continued, see previous caption for details)

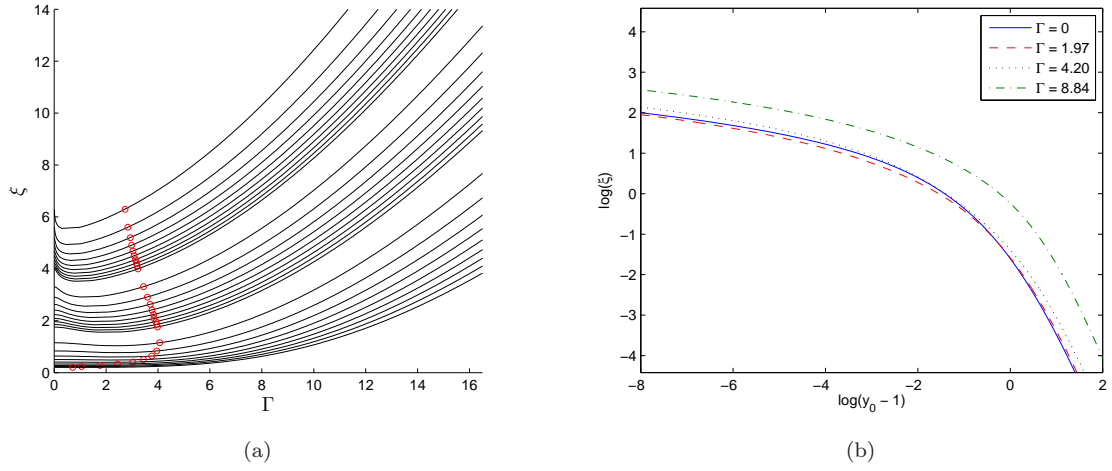
see that the total drift area exhibits a well-defined minimum which is a manifestation of the competing effects observed in Figure 4a. The smallest drift area $D = 2.93$ is achieved for $\Gamma = 1.97$, whereas for $\Gamma = 3.6$ drift area is approximately $D = \pi$, the same as in the wakeless potential flow. The particle trajectories corresponding to these two cases are shown in Figures 3b and 3c.

V. ASYMPTOTIC ANALYSIS

As was discussed in Section IV C, the drift of a particle in Föppl flow depends on two parameters, namely, the vortex circulation Γ and the initial distance y_0 between the particle and the flow centerline. In this section we derive expressions characterizing the drift when the parameters take some limiting values. The asymptotic study of the drift in the wakeless potential flow as $y_0 \rightarrow 1$ and $y_0 \rightarrow \infty$ is presented in [1], and our approach will build on this analysis.

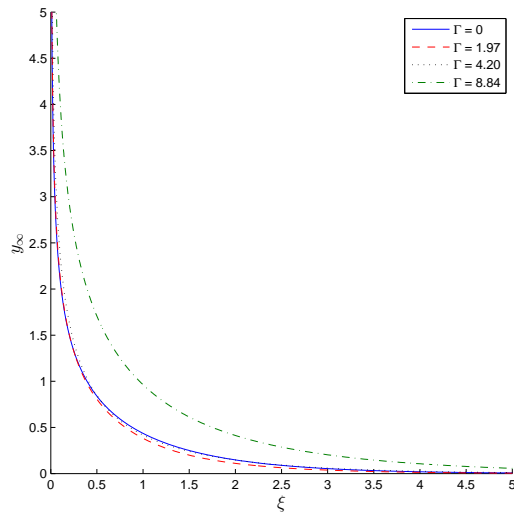
A first, trivial, observation is that in the limit $\Gamma \rightarrow 0$ the drift of the wakeless potential flow is obtained uniformly in y_0 . Here we will consider the limit $y_0 \rightarrow \infty$. Since the required transformations are rather complicated, requiring the use of symbolic algebra tools (Maple), for brevity below we will only highlight the key steps.

We start by taking the Taylor expansion of the velocity component u_x in equation (4) about the initial position of the particle $\mathbf{x}_0 = [0, y_0]^T$ and truncate it at the order $\mathcal{O}(\|\mathbf{x} - \mathbf{x}_0\|^2)$. This is justified by the observation, cf. Figure 3, that for large y_0 the particle trajectories are close to being circular and in the proximity of \mathbf{x}_0 . Our goal will be to integrate this expansion with respect to time, cf. (1), but first we have to substitute for $x(t)$ and $y(t)$ to make the expansion a function of t only. In the limit $y_0 \rightarrow \infty$ the trajectories $\mathbf{x}(t)$ can be approximated with the solutions $\tilde{\mathbf{x}}(t) = [\tilde{x}(t), \tilde{y}(t)]^T$ of system (4)



(a)

(b)



(c)

Figure 4: Dependence of drift ξ on (a) the vortex circulation Γ for initial particle positions $y_0 \in \{1.001, 1.002, \dots, 1.01, 1.02, \dots, 1.1, 1.2, \dots, 2.0\}$ (larger y_0 corresponding to lower curves), (b) the initial distance y_0 and (c) the distance y_∞ from the flow centerline measured at infinity, cf. (5), for the circulation values indicated in the legend.

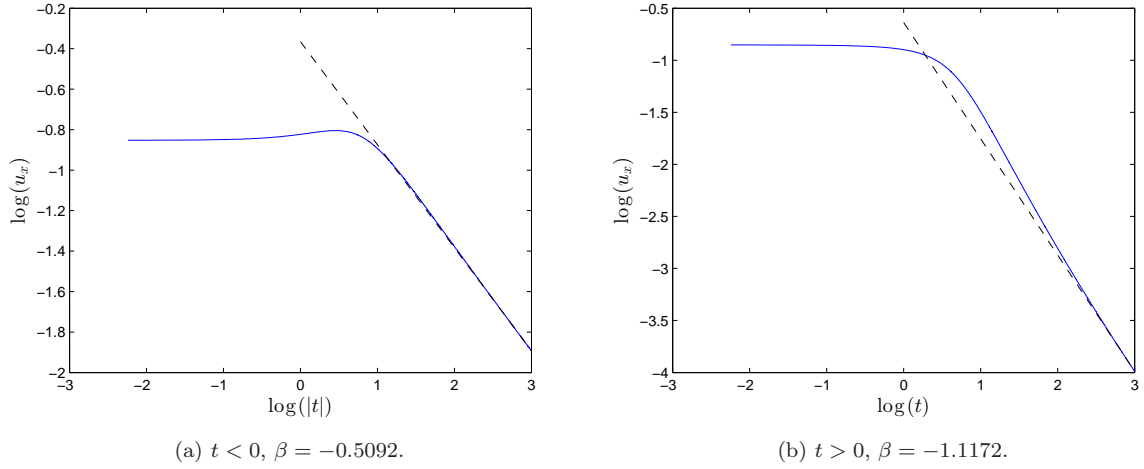


Figure 5: Behavior of the velocity component u_x following the trajectory of the particle located at $y_0 = 5$ at $t = 0$ in Kirchhoff flow for large (a) negative and (b) positive times (solid line); the dashed line represents the power-law fit (32) with the exponent values indicated in the captions.

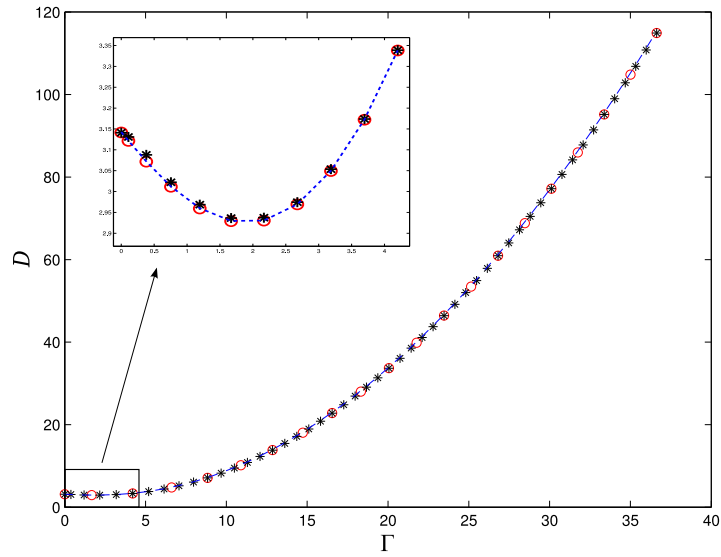


Figure 6: Total drift area D in the Föppl flows as a function of the vortex circulation Γ evaluated based on definition formula (7) (empty circles), added-mass formula (8) (crosses) and Taylor's theorem (11)–(12) (dashed line).

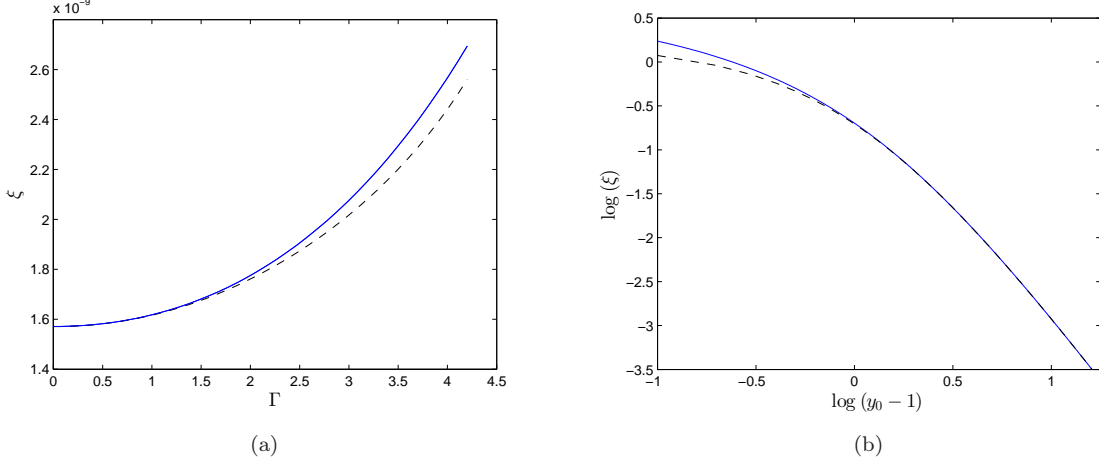


Figure 7: Dependence of drift ξ on (a) the circulation Γ for $y_0 = 1000$ and (b) the initial particle position y_0 for $\Gamma = 0.38023$; solid lines represent the actual data whereas the dashed lines correspond to asymptotic formula (37).

in which the right-hand side is evaluated at \mathbf{x}_0 , i.e., $d\tilde{\mathbf{x}}(t)/dt = \mathbf{u}([0, y_0]^T, t)$, which is written out as

$$\begin{aligned} \frac{d\tilde{x}}{dt} = & \frac{t^2 - y_0^2}{(t^2 + y_0^2)^2} + \frac{\Gamma}{2\pi} \left[-\frac{y_0 - y_1}{(-t - x_1)^2 + (y_0 - y_1)^2} + \frac{y_0 - \frac{y_1}{x_1^2 + y_1^2}}{(-t - \frac{x_1}{x_1^2 + y_1^2})^2 + (y_0 - \frac{y_1}{x_1^2 + y_1^2})^2} \right. \\ & \left. + \frac{y_0 + y_1}{(-t - x_1)^2 + (y_0 + y_1)^2} - \frac{y_0 + \frac{y_1}{x_1^2 + y_1^2}}{(-t - \frac{x_1}{x_1^2 + y_1^2})^2 + (y_0 + \frac{y_1}{x_1^2 + y_1^2})^2} \right], \end{aligned} \quad (36a)$$

$$\begin{aligned} \frac{d\tilde{y}}{dt} = & -\frac{2ty_0}{(t^2 + y_0^2)^2} + \frac{\Gamma}{2\pi} \left[\frac{-t - x_1}{(-t - x_1)^2 + (y_0 - y_1)^2} - \frac{-t - \frac{x_1}{x_1^2 + y_1^2}}{(-t - \frac{x_1}{x_1^2 + y_1^2})^2 + (y_0 - \frac{y_1}{x_1^2 + y_1^2})^2} \right. \\ & \left. - \frac{-t - x_1}{(-t - x_1)^2 + (y_0 + y_1)^2} + \frac{-t - \frac{x_1}{x_1^2 + y_1^2}}{(-t - \frac{x_1}{x_1^2 + y_1^2})^2 + (y_0 + \frac{y_1}{x_1^2 + y_1^2})^2} \right]. \end{aligned} \quad (36b)$$

Relations (36a)–(36b) are integrated analytically for $\tilde{x}(t)$ and $\tilde{y}(t)$ and, before the resulting expressions are substituted in the series expansion of u_x , they are expanded in a Taylor series with respect to Γ which is assumed small. Noting (16) and relations $y_1 = (r_1^2 - 1)/(2r_1)$ and $r_1 = \sqrt{2\sqrt{x_1^4 - x_1^2 + 1} + 2x_1^2 - 1}/\sqrt{3}$, this expansion can be re-expressed only in terms of x_1 , which is the downstream coordinate of the Föppl vortex. Finally, integrating the resulting expression from $t = -\infty$ to $t = \infty$ and keeping only the leading-order term in y_0 , we obtain the following approximation to the drift

$$\xi = \frac{\pi}{2y_0^3} [1 + 64(x_1 + 1)^4 + 192((x_1 + 1)^5 + (x_1 + 1)^6)] + \mathcal{O}((x_1 + 1)^7) \quad (37)$$

valid for $y_0 \rightarrow \infty$ and $x_1 \rightarrow -1$ (equivalently, $\Gamma \rightarrow 0$). As is evident from this relation, the presence of the Föppl vortices introduces a correction to the expression $\pi/(2y_0^3)$ characterizing the drift in the wakeless potential flow in the limit $y_0 \rightarrow \infty$ [1]. Asymptotic relation (37) is compared to the actual data for $\Gamma \rightarrow 0$ in Figure 7a and for $y_0 \rightarrow \infty$ in Figure 7b showing a very good agreement in both cases. Analysis of the drift in the presence of the Föppl vortices in the limit $y_0 \rightarrow 0$ is more complicated and is beyond the scope of the present study.

VI. DISCUSSION, CONCLUSIONS AND OUTLOOK

In this study we presented a comprehensive analysis, based on careful numerical computations supported in some regimes by asymptotic analysis, of the effects of vortex wakes on the Darwinian drift induced by steadily translating obstacles. We focused on the Föppl and Kirchhoff flows featuring, respectively, a closed and open wake, which were compared to the wakeless potential flow used as a reference. We also discussed three different approaches to the computation of the total drift area, with the method based on Taylor’s theorem leading to a decomposition of D into a “universal” part and a “flow-specific” part, in analogy with the decomposition established in [8] for the Stokes flow.

The particle trajectories in Föppl and Kirchhoff flows are quite different (cf. Figures 3b-d and 3e). In Föppl flow for certain values of Γ and y_0 the particle trajectories exhibit a secondary loop corresponding to the instant of time when the particle change direction to circumnavigate the recirculation bubble. An interesting, and perhaps somewhat unexpected, finding is that while for large values of circulation Γ the presence of the recirculation region in Föppl flow increases the total drift area, an opposite effect occurs for smaller values of Γ (Figure 4a). The increase of the total drift area for large Γ can be understood by analyzing the particle trajectories in the context of changes to the flow topology. Inspection of Figure 3a, corresponding to the wakeless potential flow, reveals that the largest displacement occurs when the particle is close to one of the stagnation points (front or rear). The presence of the wake vortices in Föppl flow introduces another stagnation point (see Figure 3b-d) in the neighborhood of which particles can be trapped and dragged for a long time. This effect is illustrated in Figure 8 where we show several particle trajectories in the neighborhood of the separation point where the boundary of the recirculation zone meets the obstacle. Symbols on the trajectories mark positions at equal time intervals, indicating that the particles closer to the separation point are trapped there for a longer time. Passage near this separation point corresponds to the climb on the second loop in the trajectories shown in Figures 3b-d. There are some interesting similarities and differences with respect to the wake effects on the drift in Stokes flows reported in [8]. In both cases the drift of an individual particle decays as y_0^{-3} when the particle’s position becomes large, cf. (37). This is a consequence of the fact that both the Föppl flow considered here and the Stokesian swimmer flow studied in [8] have a dipolar far-field representation (even though the spatial dimensions are different). On the other hand, in contrast to the behavior observed here, in the Stokes case a significant reflux (negative particle displacements) was observed resulting in a negative total drift area corresponding to large wake sizes.

We may estimate the drift area using formula (35) for cases when the size of the wake is smaller than or comparable to the size of the cylinder (which is what we may expect in many practical situations). If we consider the range $\Gamma \in [0, 7]$, we find that the relative difference between the total drift areas in the Föppl flow and in the wakeless potential flow, i.e., D and D_1 , is approximately -7% when the drift area achieves its minimum (see Figure 6) and 65% when $\Gamma \approx 7$. In Figure 9 we can see that for the representative wakes shown in Figure 3b–c, which are of relatively small size, D_1 may be a good approximation for the actual total drift area D . However, for values greater than $\Gamma \approx 4.5$, the relative difference exceeds 10% . Therefore, in practice, when attached vortices are present and are large enough, it may be useful to take into consideration their effects on the drift area. We add that, as discussed in Introduction, this analysis is based on the idealized concept of the total drift area and in practical settings, depending on the actual travel times of the obstacle, it may be advisable to consider partial drift.

In regard to Kirchhoff flow we demonstrated that drift ξ of individual particles is in fact not bounded and, consequently, the total drift area is not defined either. This finding should not be surprising, given that Kirchhoff flow has an infinite open wake (and hence can be “seen” by the particles as a moving body of an infinite extent). We note that another instance in which an unbounded total drift volume was found was the Stokes flow past a spherical droplet [37]. Since like Kirchhoff flow and in contrast to the Stokesian swimmers analyzed in [8], this flow is characterized by a *finite* drag, we may by analogy conjecture that unbounded total drift area is a feature of steady flows in unbounded domains which exhibit a nonzero drag.

We expect that the results reported here may help improve the accuracy of modeling efforts concerning biogenic mixing, such as those reported in [7]. There is a number of open questions which may deserve

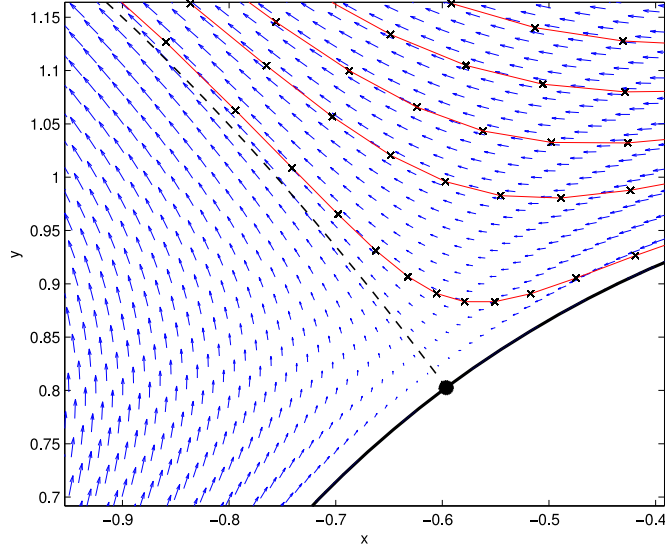


Figure 8: Neighborhood of the stagnation point (marked with a large dot) where the recirculation zone separatrix (dashed line) separates from the obstacle boundary (thick solid line). Particle trajectories are shown with thin solid lines with markers indicating positions at equal time intervals.

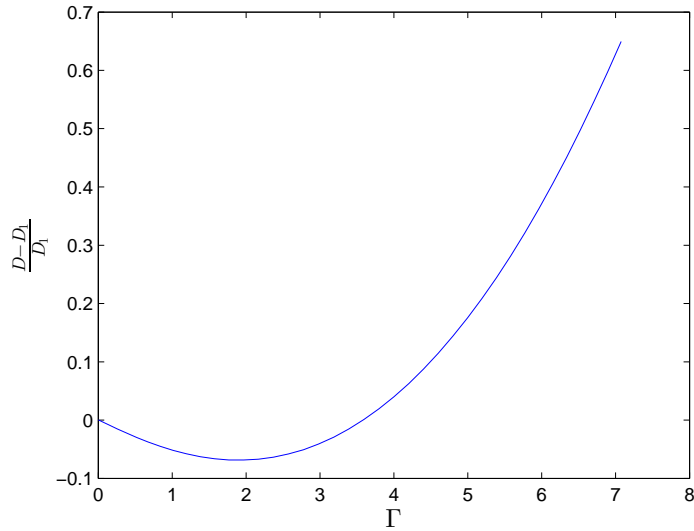


Figure 9: Relative difference between the drift area in the Föppl flow (D) and in wakeless potential flow (D_1) as a function of the circulation Γ .

further study concerning, for example, the drift induced by pairs or larger groups of moving obstacles (in the context of the potential flow theory, such flows can be studied using the formalism based on the Schottky-Klein function [38]), or obstacles with asymmetric wakes as were recently reported in [39]. The problem of identifying the shape of the obstacle which will produce a prescribed drift will lead to some interesting shape-optimization problems.

ACKNOWLEDGMENTS

The authors acknowledge the funding provided for this research through a Discovery Grant of the National Science and Engineering Research Council (NSERC) of Canada.

- [1] S. Childress. *An Introduction to Theoretical Fluid Mechanics*. Courant Lecture Notes in Mathematics. American Mathematical Society, Courant Institute of Mathematical Sciences, 2009.
- [2] I. Eames. The concept of drift and its application to multiphase and multibody problems. *Philosophical Transactions of the Royal Society A: Mathematical, Physical and Engineering Sciences*, 361:2951–2966, 2003.
- [3] J.-L. Thiffeault and S. Childress. Stirring by swimming bodies. *Physics Letters A*, 374:3487–3490, 2010.
- [4] C. Jung, T. Tél, and E. Ziemniak. Application of scattering chaos to particle transport in a hydrodynamical flow. *Chaos*, 3:555–568, 1993.
- [5] E. Ziemniak, C. Jung, and T. Tél. Tracer dynamics in open hydrodynamical flows as chaotic scattering. *Physica D*, 76:123–146, 1994.
- [6] W. H. Munk. Abyssal recipes. *Deep-Sea Research*, 13:707–730, 1966.
- [7] K. Katija and J. O. Dabiri. A viscosity-enhanced mechanism for biogenic ocean mixing. *Nature*, 460:624–626, 2009.
- [8] D. O. Pushkin, H. Shum, and J. M. Yeomans. Fluid transport by individual microswimmers. *Journal of Fluid Mechanics*, 726:5–25, 2013.
- [9] J. Clerk-Maxwell. On the displacement in a case of fluid motion. *Proceedings of the London Mathematical Society*, 3:82–87, 1870.
- [10] L. M. Milne-Thomson. *Theoretical Hydrodynamics*. Dover, 1968.
- [11] Raph Levien. The elastica: a mathematical history. Technical Report UCB/EECS-2008-103, EECS Department, University of California, Berkeley, Aug 2008. URL <http://www.eecs.berkeley.edu/Pubs/TechRpts/2008/EECS-2008-103.html>.
- [12] Ch. Darwin. Note on hydrodynamics. *Mathematical Proceedings of the Cambridge Philosophical Society*, 49:342–354, 1953.
- [13] C.-S. Yih. New derivations of Darwin’s theorem. *Journal of Fluid Mechanics*, 152:163–172, 1985.
- [14] T. B. Benjamin. Note on added mass and drift. *Journal of Fluid Mechanics*, 169:251–256, 1986.
- [15] C.-S. Yih. Evolution of Darwinian drift. *Journal of Fluid Mechanics*, 347:1–11, 1997.
- [16] I. Eames, S. E. Belcher, and J. C. R. Hunt. Drift, partial drift and Darwin’s proposition. *Journal of Fluid Mechanics*, 275:201–223, 1994.
- [17] J. Bataille, M. Lance, and J. L. Marie. Some Aspects of the Modeling of Bubbly Flows. In G. F. Hewitt, F. Mayinger, and J. R. Riznic, editors, *Phase-interface phenomena in multiphase flow*, Proceedings of the International Centre for Heat and Mass Transfer, pages 179–193. Hemisphere Pub. Corp., New York, 1991.
- [18] I. Eames and M. E. McIntyre. On the connection between Stokes drift and Darwin drift. *Mathematical Proceedings of the Cambridge Philosophical Society*, 126:171–174, 1999.
- [19] J. O. Dabiri. Note on the induced Lagrangian drift and added-mass of a vortex. *Journal of Fluid Mechanics*, 547:105–113, 2006.
- [20] Z. Lin, J.-L. Thiffeault, and S. Childress. Stirring by squirmers. *Journal of Fluid Mechanics*, 669:167–177, 2011.
- [21] R. Camassa, R. M. McLaughlin, M. N. J. Moore, and A. Vaidya. Brachistochrones in potential flow and the connection to Darwin’s theorem. *Physics Letters A*, 372:6742–6749, 2008.
- [22] G. I. Taylor. The energy of a body moving in an infinite fluid, with an application to airships. *Proceedings of the Royal Society A*, 120:13, 1928.
- [23] L. Landweber and C.-S. Yih. Forces, moments, and added masses for rankine bodies. *Journal of Fluid Mechanics*, 1:319–336, 1956.
- [24] V. V. Sychev, A. I. Ruban, V. V. Sychev, and G. L. Korolev. *Asymptotic Theory of Separated Flows*. Cambridge University Press, 1998.
- [25] L. Föppl. Wirbelbewegung hinter einem Kreiscylinder. *Sitzb. d. k. Bayr. Akad. d. Wiss.*, 1:1–17, 1913.
- [26] A. Elcrat, B. Fornberg, M. Horn, and K. Miller. Some steady vortex flows past a circular cylinder. *J. Fluid Mech.*, 409:13–27, 2000.
- [27] B. Protas. Higher-order Föppl models of steady wake flows. *Physics of Fluids*, 11:117109, 2006.

- [28] S. Tang and N. Aubry. On the symmetry breaking instability leading to vortex shedding. *Phys. Fluids*, 9: 2550–2561, 1997.
- [29] F. Li and N. Aubry. Feedback control of a flow past a cylinder via transverse motion. *Physics of Fluids*, 15:2163–2176, 2003.
- [30] B. Protas. Linear feedback stabilization of laminar vortex shedding based on a point vortex model. *Physics of Fluids*, 16:4473–4488, 2004.
- [31] B. Protas. Center manifold analysis of a point-vortex model of vortex shedding with control. *Physica D*, 228:179–187, 2007.
- [32] B. Protas. Vortex dynamics models in flow control problems. *Nonlinearity*, 21:R203–R250, 2008. doi: 10.1088/0951-7715/21/9/R01. (invited paper).
- [33] T. Levi-Civita. Scie e leggi di reistenza. *Rendiconti del Circolo Matematico di Palermo*, XXIII:1–37, 1907.
- [34] S. Brodetsky. Discontinuous fluid motion past circular and elliptic cylinders. *Proceedings of the Royal Society of London. Series A*, 102:542–553, 1923.
- [35] IEEE Computer Society. Ieee standard for floating-point arithmetic, August 2008. IEEE. doi:10.1109/IEEESTD.2008.4610935.
- [36] See supplementary material at (URL to be supplied by AIP) for animated versions of particle trajectories in wakeless potential, Föppl and Kirchhoff flows.
- [37] I. Eames, D. Gobby, and S. B. Dalziel. Fluid displacement by Stokes flow past a spherical droplet. *Journal of Fluid Mechanics*, 485:67–85, 2003.
- [38] D.G. Crowdy. Analytical solutions for uniform potential flow past multiple cylinders. *Eur. J. Mech. B/Fluids*, 25:459–470, 2006.
- [39] A. Elcrat, M. Ferlauto, and L. Zannetti. Point vortex model for asymmetric inviscid wakes past bluff bodies. *Fluid Dynamics Research*, 46:031407, 2014.